


**Boosting biomolecular switch efficiency with quantum coherence**

Mattheus Burkhard

*Clarendon Laboratory, University of Oxford, Parks Road, Oxford OX1 3PU, United Kingdom  
and Département de Physique, École Normale Supérieure Paris-Saclay, 4 Av. des Sciences, 91190 Gif-sur-Yvette, France*Onur Pusuluk *Faculty of Engineering and Natural Sciences, Kadir Has University, Fatih, Istanbul, Türkiye*

Tristan Farrow\*

*Clarendon Laboratory, University of Oxford, Parks Road, Oxford OX1 3PU, United Kingdom  
and NEOM University, and Education, Research, Innovation Foundation, Tabuk 49643-9136, Saudi Arabia*

(Received 8 November 2023; accepted 22 April 2024; published 1 July 2024)

The resource theory of quantum thermodynamics has emerged as a powerful tool for exploring the out-of-equilibrium dynamics of microscopic and highly correlated systems. Recently, it has been employed in photoisomerization, a mechanism facilitating vision through the isomerism of the photoreceptor protein rhodopsin, to elucidate the fundamental limits of efficiency inherent in this physical process. Limited attention has been given to the impact of energetic quantum coherences in this process, as these coherences do not influence the energy-level populations within an individual molecule subjected to thermal operations. However, a specific type of energetic quantum coherences can impact the energy-level populations in the scenario involving two or more molecules. In this study, we examine the case of two molecules undergoing photoisomerization to show that energetic quantum coherence can function as a resource that amplifies the efficiency of photoisomerization. These insights offer evidence for the role of energetic quantum coherence as a key resource in the realm of quantum thermodynamics at mesoscopic scales.

DOI: [10.1103/PhysRevA.110.012411](https://doi.org/10.1103/PhysRevA.110.012411)**I. INTRODUCTION**

Thermodynamics and quantum mechanics represent distinct disciplines that grapple with discrepancies between their fundamental principles. The emerging field of quantum thermodynamics [1–4] bridges these two disciplines by proposing innovative strategies to reconcile them. One of the main discrepancies lies in the interpretation of energy within these two domains. The first law of thermodynamics traditionally characterizes an additive decomposition of energy into work and heat. In quantum mechanics, however, while energy is a measurable quantity, there are no directly observable counterparts for heat and work. By adopting a dynamical approach [5] based on open quantum systems theory [6], quantum thermodynamics can precisely define and quantify heat and work within quantum systems.

Thermodynamic quantities such as free energy are well defined only in equilibrium conditions, and in the limit of identical and independent distributions the conventional laws of thermodynamics hold true. Nonetheless, the intricate na-

ture of quantum systems complicates matters. Unlike classical systems, we can only clone quantum systems with prior knowledge [7], and the presence of quantum coherence often pushes these systems far from equilibrium. Quantum correlations complicate the picture further by preventing quantum systems from becoming independent. To tackle these steep challenges, quantum thermodynamics employs information-theoretic approaches [8–11] falling under the framework known as quantum resource theories [12,13]. These approaches differentiate between states that are accessible by thermodynamical processes and those that are not.

The insight that heat and quantum coherence are convertible represents a significant advance in the realm of quantum thermodynamics [14–19]. Specifically, a form of energetic quantum coherence responsible for generating heat arises through the dynamical framework rooted in open quantum systems theory [20–24]. This specific manifestation of coherence is characterized by superpositions within degenerate energy states and has led to various nomenclatures such as “heat-exchange coherence,” [20,21] “internal coherence,” [22] or “horizontal coherence” [23,24]. This kind of coherence has enabled the establishment of a quantum Onsager relation that links coherence flow and heat flow [25].

The information-theoretical approach refers to the same type of coherence as “zero-mode coherence.” In this framework [26–28], one considers zero-mode coherences in conjunction with the energy-level populations within the thermomajorization criterion (an extension of the second law of

\*Contact author: [tristan.farrow@cantab.net](mailto:tristan.farrow@cantab.net)

*Published by the American Physical Society under the terms of the Creative Commons Attribution 4.0 International license. Further distribution of this work must maintain attribution to the author(s) and the published article’s title, journal citation, and DOI.*

thermodynamics [10]). While the study of coherence in thermal processes within the framework of open quantum systems has garnered significant attention, by comparison, the study of their effects within resource theories remains relatively uncharted territory. Our work aims to fill this gap.

We consider the process of photoisomerization to illustrate how these principles can usefully be applied. Photoisomerization—or photoswitching—stands as an example of the explanatory capacity of the thermomajorization criterion in elucidating the behavior of systems far from equilibrium such as biological molecules [29]. The same model system has also been used to identify contributions from non-Markovianity in thermomajorization [30]. In Ref. [29] the probability of extracting work from zero-mode coherence in a molecular pair was also examined. However, in both prior studies, the investigation of photoisomerization efficiency focused solely on a single photoswitching molecule where the contributions of coherence to the efficiency cannot be examined since in a single-molecule system the zero-mode quantum coherence is absent. Here, we explore a scenario where two identical rhodopsin molecules are simultaneously stimulated by a single photon. For example, this can be achieved using a beam splitter scheme like the one presented in Sec. IV. Such single-photon excitations lead to the sharing of zero-mode coherence between the molecules and giving rise to nontrivial contributions of coherence to the final state of the reaction.

## II. RESOURCE THEORY

### A. Defining possible operations

In one quantum-thermodynamic model, free operations at inverse temperature  $\beta = 1/k_B T$  are called *thermal operations*. These operations do not require any additional resources (no external ‘battery’) and can be [10,13]

- (i) contact with a thermal bath B (free use of states with a density matrix  $\rho_B = e^{-\beta H_B}/Z$ ).
- (ii) any energy-preserving global unitary transformation  $U$  on the whole system.
- (iii) tracing out any subsystem, and in particular the bath B.

This means that the thermal operation from a certain initial state  $\rho$  to a final state  $\sigma$  can be described by the functional  $\mathcal{T}$ :

$$\mathcal{T}[\rho] = \text{Tr}_B[U(\rho \otimes \rho_B)U^\dagger] = \sigma. \quad (1)$$

In other words a thermal operation on a system  $\rho$  is any process that only takes thermal energy from the bath and preserves the total energy.

### B. Constructing a Lorenz curve

Now, let us define thermomajorization. It is a mathematical tool that allows us to determine the relative ordering of states based on their energy distributions. When one thermal state thermomajorizes another, it means that the former has a more organized and concentrated energy distribution compared with the latter. It resembles the second law of thermodynamics where organized systems have lower entropy than those where the energy is distributed over all degrees of freedom. The thermomajorization relation is important in

resource theory as it helps quantify the usefulness or value of states for performing certain thermodynamic tasks.

$H = \sum_j E_j |j\rangle\langle j|$  denotes the Hamiltonian that governs the mechanics of our system. Its state is represented by a density matrix  $\rho$  whose diagonal elements are  $\rho_{jj}|j\rangle\langle j|$ . The coefficients can be regrouped in what is called a population vector:

$$\begin{aligned} \vec{p} &= (\rho_{11}, \rho_{22}, \dots, \rho_{dd}) \\ &\equiv (p_1, p_2, \dots, p_d). \end{aligned} \quad (2)$$

It contains the probabilities to be in one of the energy eigenstates, with  $\sum_j^d p_j = \text{Tr}(\rho) = 1$ . To explain thermomajorization we need to define a curve for this state called the Lorenz curve and denoted by  $L(\vec{p})$ . We can construct this curve with a procedure that includes two main steps. First, one has to calculate the rescaled coefficients  $p_j e^{\beta E_j}$ , and order them from greatest to least:

$$p_{j'} e^{\beta E_{j'}} \leq p_{k'} e^{\beta E_{k'}}, \quad \text{for all } j' > k'. \quad (3)$$

Second, one has to consider the points

$$\left( \sum_{j=1}^{\alpha} e^{-\beta E_j}, \sum_{j=1}^{\alpha} p_j \right), \quad \text{with } \alpha = 1, 2, \dots, d. \quad (4)$$

Connecting them with straight lines beginning at the origin defines a piecewise-linear curve, the Lorenz curve. The  $x$  coordinates run from zero to  $Z$ , the partition function  $Z = \sum_i^d e^{-\beta E_i}$ . The  $y$  coordinates go from zero to one, the sum of all probabilities.

Now let us say  $(\sigma, H')$  defines another state with a population vector  $\vec{q} = (q_1, \dots, q_{d'})$ . If the  $(\rho, H)$  curve lies above or on the  $(\sigma, H')$  curve, then  $(\rho, H)$  is said to thermomajorize  $(\sigma, H')$ . This can be denoted by

$$[L(\vec{p})](x) \geq [L(\vec{q})](x) \quad \forall x \in [0, Z],$$

$$\text{shorthand notation: } L(\vec{p}) \geq L(\vec{q}). \quad (5)$$

A mathematical theorem [10,27,31] links thermal operations to thermomajorization. For two quasiclassical states  $\rho$  and  $\sigma$ , if and only if  $(\rho, H)$  thermomajorizes  $(\sigma, H')$  there exists some thermal operation  $\mathcal{T}$  that maps  $\rho$  to  $\sigma$ . In other terms, if  $\rho$  ( $\sigma$ ) has a population vector  $\vec{p}$  ( $\vec{q}$ ), then

$$[L(\vec{p}) \geq L(\vec{q})] \iff (\exists \mathcal{T}, \mathcal{T}[\rho] = \sigma). \quad (6)$$

### C. Importance of off-diagonal elements (coherences)

The density matrix  $\rho$  of a system can be written as the sum of its elements in the energy eigenbasis

$$\rho = \sum_{n,m} \rho_{nm} |n\rangle\langle m|, \quad (7)$$

where  $n$  designates an eigenstate whose (possibly degenerate) energy can be expressed as  $E_n$ . The transition frequency between states  $\omega = (E_n - E_m)/\hbar$  defines a mode. All elements  $\rho_{nm}$  with the same transition energy belong to the same  $\omega$  mode:

$$\rho^{(\omega)} \equiv \sum_{n,m} \rho_{nm} |n\rangle\langle m|. \quad (8)$$

This way the density matrix can be decomposed in its  $\omega$  modes,

$$\rho = \sum_{\omega} \rho^{(\omega)}. \quad (9)$$

One can prove that these  $\omega$  modes evolve independently using the time-translation symmetry of thermal operations. This symmetry is defined by (more on this in Refs. [10,13])

$$\mathcal{T}[e^{-iHt/\hbar} \rho e^{iHt/\hbar}] = e^{-iHt/\hbar} \mathcal{T}[\rho] e^{iHt/\hbar}. \quad (10)$$

The claim is that  $\mathcal{T}[\rho^{(\omega)}]$  is also an  $\omega$  mode.

$$\begin{aligned} e^{-iHt/\hbar} \mathcal{T}[\rho^{(\omega)}] e^{iHt/\hbar} &= \mathcal{T}[e^{-iHt/\hbar} \rho^{(\omega)} e^{iHt/\hbar}] \\ &= \mathcal{T}[e^{-i\omega t} \rho^{(\omega)}] \\ &= e^{-i\omega t} \mathcal{T}[\rho^{(\omega)}]. \end{aligned} \quad (11)$$

This claim holds, which shows that all  $\omega$  modes of a density matrix evolve independently during a thermal operation. For a nondegenerate system the only elements  $\rho_{nm}$  where  $\omega_n - \omega_m = 0$  are the diagonal elements. This is why in certain cases we can neglect the impact of the off-diagonal elements in thermomajorization.

In previous studies of photoisomerization using thermomajorization [29,30], the model only involved a nondegenerate energy eigenbasis. This explains why it was not previously necessary to consider coherences in the calculations.

For a system with degenerate energies one has to include the off-diagonal elements in the thermomajorization procedure. The method described below was presented in Refs. [27,28]:

$$\rho \xrightarrow{\mathcal{U}} \rho^* \xrightarrow{\mathcal{T}} \sigma^* \xrightarrow{\mathcal{U}^\dagger} \sigma.$$

First one diagonalizes the initial density matrix  $\rho$  with a unitary transformation  $\mathcal{U}$ . In fact  $\rho$  restricted to its zero modes is already block-diagonal in the energy-eigenbasis, so  $\mathcal{U}$  will act on the blocks of degenerate energy subspaces. This transformation is allowed because energy-preserving unitaries are free and acting on subspaces of constant energy preserves the energy. We obtain  $\rho^*$  where all the zero modes are on the diagonal. So we have a new initial population vector  $\vec{p}_i^*$  on which to apply the thermomajorization procedure  $\mathcal{T}$ . This gives us a final state  $\sigma^*$  and we can apply the inverse transformation  $\mathcal{U}^\dagger$  to switch back to the original basis and get our final result  $\sigma$ . This is an innovative method for studying coherences and quantifying their effects on photoisomerization.

### III. MODEL OF PHOTOISOMERIZATION

Thermomajorization can give us the optimal quantum thermodynamical yield of a given process. One goal of this work is to complete our understanding of the quantum yield of a molecule undergoing photoisomerization. Also called photoswitching, it is triggered in certain molecules when they absorb a photon, the acquired energy induces a rotation around one of the molecule's carbon double bonds. As for example with the protein rhodopsin, the molecule switches from a *cis* to *trans* configuration when it absorbs a photon [32–34]. Rhodopsin is a protein responsible for vision in human and animal retinas, by photoisomerizing it transforms the optical signal into a chemical chain reaction which transmits

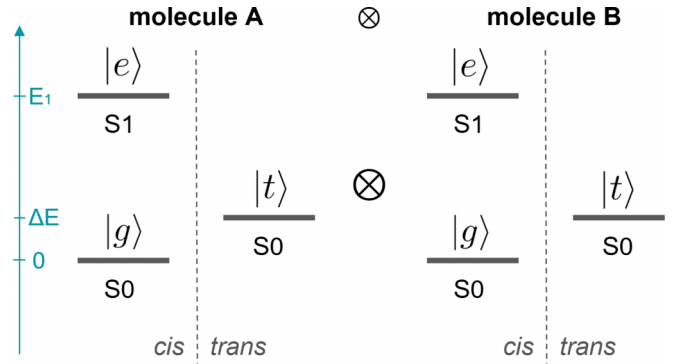


FIG. 1. A simplified picture of the energy levels of two molecules. The full energy eigenbasis consists of  $\{|i\rangle \otimes |j\rangle\}$  with  $i, j \in \{e, g, t\}$ .

a signal to the brain. The resource-theoretical method for the case of a single molecule undergoing photoisomerization was developed in Refs. [29,30]. The total Hamiltonian presented in Eq. (12) is restricted to the evolution of the molecule along the reaction coordinate of the chemical transformation which is the angle of rotation  $\phi$  around the double bond. Similar models have been developed for different biosystems [35]:

$$H = \int_{\phi=0}^{\pi} H_{\text{mol}}(\phi). \quad (12)$$

In fact, by focusing on the initial and final state,  $\phi = 0$  or  $\pi$ , we can ignore the intermediate states and energy barriers when we want to obtain the optimal possible yield allowed by thermal operations. This is justified in the context of resource theory that answers the question of whether a certain transformation is possible or not. The theory makes general statements about complex dynamics and this applies to studying the efficiency of photoisomerization. The process can be seen as the evolution of an effective three-level system. As shown in Fig. 1 for one molecule (A or B) these states are called  $\{|g\rangle; |e\rangle; |t\rangle\}$ . They correspond to the electronic *ground* and *excited* states of the molecular *cis* configuration, and the *trans* ground state. The omission of the *trans* excited state can be justified by saying that it does not impact the final population in  $|t\rangle$ . If a molecule reaches the *trans* excited state, it can freely relax into the corresponding ground state and emit its surplus of energy into the bath  $B$ . Here, the bath is a general description of the molecule's vibrational degrees of freedom and its interactions with the environment. The total molecular state is encoded by a density matrix whose diagonal elements form a population vector  $\vec{p} = (p_g, p_e, p_t)$ . It corresponds to the energy eigenbasis restricted to  $\phi = 0$  and  $\pi$ . The off-diagonal elements of the density matrix cannot influence the quantum yield in such a system, as explained in Refs. [10,13]. Indeed the energy eigenbasis is nondegenerate, with  $\Delta E$  describing the energy gap from *cis* to *trans* and  $E_1$  the energy of the photoexcitation (see Fig. 1). Typical values in the case of photoisomerization of rhodopsin are  $E_1 = 2.48\text{eV}$  and  $\Delta E = 1.39\text{eV}$  [33,34,36,37]. In this case the diagonal elements are the only zero modes, so coherences do not affect their evolution.

When describing photoisomerization, the initial conditions correspond to the photoabsorption event. The initial population vector is a mixture of the *cis* ground state  $S_0$  and its first-excited state  $S_1$  with  $p$  being the probability of photoexcitation:

$$\vec{p}_i = (1 - p, p, 0). \quad (13)$$

The final state can be described by any combination  $\vec{q} = (q_g, q_e, q_t)$  as long as there is a thermal operation that maps it to the initial one. That means that  $\vec{q}$  is thermomajorized by  $\vec{p}_i$ , or in mathematical terms  $L(\vec{p}_i) \geq L(\vec{q})$ .

Let us expand the model to  $N = 2$  molecules, because coherences will start to play a role due to degeneracy. The three-level approximation leads to an overall dimension of  $3^N = 3^2 = 9$ , which complicates calculations and increases computational cost.

To characterize thermodynamic properties such as energy, heat, work, and temperature at a local level within a joint system, it is essential to describe the system in terms of its local energy eigenstates. In systems involving photoisomers, where different molecular configurations can interact, the total Hamiltonian reads

$$H = H_A \otimes I_B + I_A \otimes H_B + V_{AB}. \quad (14)$$

Here,  $H_A$  and  $H_B$  correspond to the Hamiltonians of the individual molecules,  $I_A$  and  $I_B$  denote identity operators, and  $V_{AB}$  signifies the interaction between the components. To adequately capture the local thermodynamic properties, we should represent the molecular state and the total Hamiltonian in the eigenbasis of  $H_A \otimes I_B + I_A \otimes H_B$ .

The pure state of the two molecules can be described as a sum of combinations of basis states ( $g$ ,  $e$  and  $t$ ):

$$|\psi\rangle = \sum_{i,j \in \{g,e,t\}} \alpha_{ij} |i\rangle \otimes |j\rangle, \quad (15)$$

$$\text{or } |\psi\rangle = \sum_{i,j \in \{g,e,t\}} \alpha_{ij} |ij\rangle. \quad (16)$$

For thermomajorization, the initial state in the photoisomerization process is given by the population vector that describes the occupation probabilities in the *cis* subspace  $\{gg, ge, eg, ee\}$ :

$$\vec{p}_i = (p_{gg}, p_{ge}, p_{eg}, p_{ee}, 0, 0, 0, 0, 0), \quad (17)$$

where  $\sum_{i,j \in \{g,e\}} p_{ij} = 1$ . Indeed, the probabilities of having some molecule in  $|t\rangle$  are approximately zero before the photoisomerization. Afterwards the final state can be any  $\vec{q} = (q_{gg}, q_{ge}, q_{eg}, q_{ee}, q_{gt}, q_{tg}, q_{et}, q_{te}, q_{tt})$  as long as  $L(\vec{p}_i) \geq L(\vec{q})$ . The optimal quantum yield can be defined as the sum of probabilities where any of the two molecules has reached the *trans* state, which means that at least one of them is in  $t$ :

$$QY_{\text{any}} \equiv \max_{L(\vec{p}_i) \geq L(\vec{q})} \sum_{i \in \{g,e\}} (q_{it} + q_{ti}) + q_{tt}. \quad (18)$$

Another possible definition of the quantum yield is

$$QY_{\text{both}} \equiv \max_{L(\vec{p}_i) \geq L(\vec{q})} q_{tt}, \quad (19)$$

when both have reached the *trans* state.

For two molecules there is a degeneracy,  $E_{ge} = E_{eg} = E_1$ , two different two-molecule states  $|ge\rangle$  and  $|eg\rangle$  correspond to

this energy. And  $\rho|_{E_1}$  is the density matrix restricted to this subspace of energy  $E_1$  containing the states where exactly one of the two molecules is excited at  $E_1$  while the remaining one is in the ground state. The initial state does not have to be a pure state, so we can consider a mixed state, where some off-diagonal coefficients are set by a parameter  $\lambda$ :

$$\rho|_{E_1} = \begin{pmatrix} |\alpha_{ge}|^2 & \lambda \\ \bar{\lambda} & |\alpha_{eg}|^2 \end{pmatrix} \equiv \begin{pmatrix} p_{ge} & \lambda \\ \bar{\lambda} & p_{eg} \end{pmatrix}, \quad (20)$$

with  $0 \leq |\lambda| \leq \sqrt{p_{eg}p_{ge}}$ . This parameter encodes the amount of decoherence the state has experienced. This is reflected in a loss of purity:

$$\text{Tr}(\rho|_{E_1}^2) = p_{ge}^2 + 2|\lambda|^2 + p_{eg}^2 \leq (p_{ge} + p_{eg})^2. \quad (21)$$

After diagonalizing this mixed state one obtains

$$\rho^*|_{E_1} = \begin{pmatrix} p_+ & 0 \\ 0 & p_- \end{pmatrix}, \quad (22)$$

$$\text{with } p_{\pm} = \frac{p_{ge}^2 + p_{eg}^2}{2} \pm \sqrt{\left(\frac{p_{ge}^2 - p_{eg}^2}{2}\right)^2 + |\lambda|^2}. \quad (23)$$

This gives us an updated version of the probability vector introduced in Eq. (17) in the presence of decoherence:

$$\vec{p}_i^* = (p_{gg}, p_+, p_-, p_{ee}, 0, 0, 0, 0, 0). \quad (24)$$

The unitary conserves the global probability to be in the  $E_1$  subspace  $p_+ + p_- = p_{ge} + p_{eg}$ .

#### IV. RESULTS AND DISCUSSION

One can imagine the following thought experiment to study coherence effects. An incoming photon goes through a first beam splitter that transmits only a portion  $p$  of its wave function. That portion is then guided towards a perfect 50 : 50 beam splitter and ends up in a state of superposition across paths A and B. So there is a probability  $1 - p$  that the photon will be in neither A nor B, and a probability  $p/2$  to be respectively in A or B exclusively. After the beam splitter the photonic state is

$$|\gamma\rangle = \sqrt{1-p}|A : 0, B : 0\rangle + \sqrt{\frac{p}{2}}(|A : 1, B : 0\rangle + |A : 0, B : 1\rangle), \quad (25)$$

where 1 and 0 encode the presence and absence of the photon in the path A or B. In each path there is a photoisomerizable molecule, also respectively called A and B. Now,  $p$  is—as in Eq. (13)—analogous to the probability that the molecule absorbs the photon, one obtains the following two-molecular state:

$$|\psi\rangle = \sqrt{1-p}|A : g, B : g\rangle + \sqrt{\frac{p}{2}}(|A : e, B : g\rangle + |A : g, B : e\rangle). \quad (26)$$

The density matrix, restricted to its zero modes, can be written in a simpler form as

$$\rho = (1-p)|gg\rangle\langle gg| + \frac{p}{2}(|ge\rangle + |eg\rangle)(\langle ge| + \langle eg|). \quad (27)$$

Restricted to the initial subspace of excited and ground state of the *cis* configuration, one obtains the following matrix representation:

$$\rho|_{e,g} = \begin{pmatrix} 1-p & 0 & 0 & 0 \\ 0 & p/2 & p/2 & 0 \\ 0 & p/2 & p/2 & 0 \\ 0 & 0 & 0 & 0 \end{pmatrix}. \quad (28)$$

There are now two off-diagonal which are also zero modes appearing in the initial configuration. Their presence will impact the final quantum yield.

Now, if we assume that the process described so far is not taking place in a closed system, then some decoherence can take place. The off-diagonal elements will be subjected to it and their amplitude may vary. In particular we can replace the coherence with a parameter  $\lambda$ , such that

$$\tilde{\rho}|_{e,g} = \begin{pmatrix} 1-p & 0 & 0 & 0 \\ 0 & p/2 & \lambda & 0 \\ 0 & \bar{\lambda} & p/2 & 0 \\ 0 & 0 & 0 & 0 \end{pmatrix}, \quad (29)$$

with  $0 \leq |\lambda| \leq p/2$ . When diagonalized,

$$\tilde{\rho}^*|_{e,g} = \begin{pmatrix} 1-p & 0 & 0 & 0 \\ 0 & p/2 + |\lambda| & 0 & 0 \\ 0 & 0 & p/2 - |\lambda| & 0 \\ 0 & 0 & 0 & 0 \end{pmatrix}. \quad (30)$$

This gives us the following initial population vector:

$$\begin{aligned} \tilde{p}_i^* &= \{1-p, p/2 + |\lambda|, p/2 - |\lambda|, 0, 0, 0, 0, 0\} \\ &\equiv \tilde{p}_{\text{sup}}(p, \lambda), \end{aligned} \quad (31)$$

called  $\tilde{p}_{\text{sup}}$  for *superposition* of molecular excitations.

Now we can study the influence of the coherence parameter  $\lambda$  on the photoisomerization efficiency using thermomajorization.

For the following figures, the typical parameters for rhodopsin ( $E_1 = 2.48$  eV and  $\Delta E = 1.39$  eV) were used. We also rescaled the inverse temperature to be  $\beta = 1$  eV<sup>-1</sup>. For the initial  $\tilde{p}_{\text{sup}}$ , we used  $p = 0.7$  and compared low coherence ( $\lambda = 0.02$ ) and high coherence ( $\lambda = 0.2$ ) regimes.

As shown in Fig. 2 the latter case has a slightly increased Lorenz curve in the range between zero and 0.25 on the horizontal axis. This feature can be understood with the following argument: For the initial population vector  $\tilde{p}_{\text{sup}}$ , we have  $p_{\pm} = p/2 \pm |\lambda|$ . When constructing the Lorenz curve  $L(\tilde{p}_i)$ , the population vector has to be reordered, and the resulting vector can be called  $\tilde{p}_i'$ . For all values of  $\lambda$ ,  $p_+$  will be ordered before  $p_-$ , because  $p_+ e^{\beta E_1} > p_- e^{\beta E_1}$ , and let us say for simplicity that they end up being adjacent at positions  $k+1$  and  $k+2$ . This means that there are  $k$  other terms in  $\tilde{p}_i'$  before  $p_+$  and  $p_-$ . This is in fact the case in Fig. 2 and here  $k = 1$  [there is only one data point preceding  $p_+$  and  $p_-$ , the origin (0,0)]. Now, the point  $k+1$  of the Lorenz curve will take the value given below on its y axis:

$$\sum_{j=1}^k (\tilde{p}_i')_j + p_+ = \sum_{j=1}^k (\tilde{p}_i')_j + p/2 + |\lambda|. \quad (32)$$

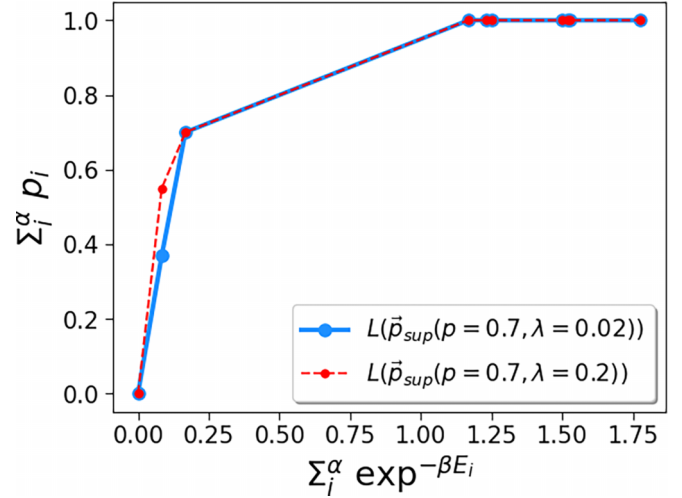


FIG. 2. Comparison of Lorenz curves of initial states with differing coherence, but same  $p = 0.7$ . High-coherence state  $\tilde{p}_{\text{sup}}(\lambda = 0.2)$  has a higher curve than low-coherence state  $\tilde{p}_{\text{sup}}(\lambda = 0.02)$ . Coherence leads to higher thermomajorization potentiality.

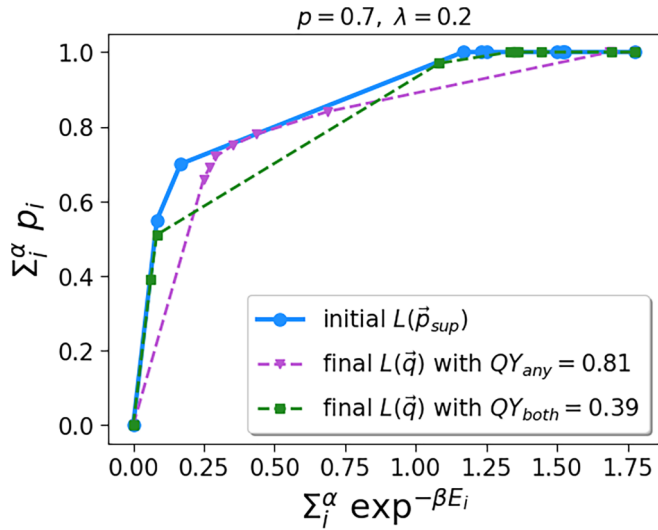
The higher the coherence parameter  $\lambda$ , the higher the Lorenz curve  $L(\tilde{p}_{\text{sup}}(p, \lambda))$  at this point. The next data point, numbered  $k+2$ , has the y coordinate

$$\sum_{j=1}^k (\tilde{p}_i')_j + p_+ + p_- = \sum_{j=1}^k (\tilde{p}_i')_j + p. \quad (33)$$

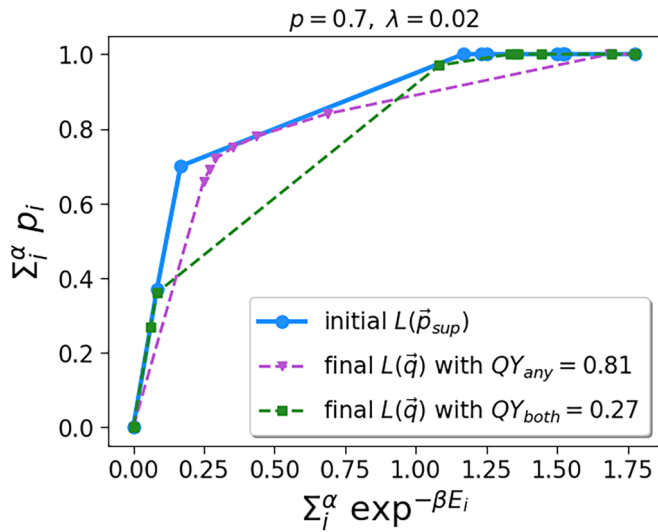
This result does not depend on  $\lambda$  because we always have  $p_+ + p_- = p_{ge} + p_{eg}$ . So, whatever the value of  $\lambda$ , the Lorenz curve reaches the same height after  $k+2$  points. Hence, by increasing  $\lambda$  we obtain higher Lorenz curves with increasing convexity. This is shown by the red dotted line above the blue one in Fig. 2,  $L(\tilde{p}_{\text{sup}}(p = 0.7, \lambda = 0.2)) \geq L(\tilde{p}_{\text{sup}}(p = 0.7, \lambda = 0.02))$ .

The increase in coherence leads to higher quantum yields, see Fig. 3. The higher the initial Lorenz curve, the more states are thermomajorized by it so it can allow higher final occupation probabilities. Indeed  $QY_{\text{both}} = 0.39$  when  $\lambda = 0.2$  [Fig. 3(a)] but only  $QY_{\text{both}} = 0.27$  when  $\lambda = 0.02$  [Fig. 3(b)]. There is a significant net increase from 27% to 39%. The Lorenz curves of these final optimal states are shown in green dashed. They are expectedly both below the initial blue line, because the final states are thermomajorized by  $\tilde{p}_{\text{sup}}(p, \lambda)$ .

Let us consider the role of coherence in this increase from 27% to 39%. If one tries to find the final state with the best quantum yield  $QY_{\text{both}}$ , by definition one has to construct the optimal Lorenz curve that is below the initial blue curve in Fig. 3 and that maximizes  $q_{tt}$ . A maximal  $q_{tt}$  will likely end up in first place in the reordering of elements [see Eq. (3)]. This gives us the first data point (after the origin) of  $L(\tilde{q})$ :  $(e^{-\beta E_{tt}}, q_{tt})$ . It has to be below the blue line, because  $L(\tilde{p}_i) \geq L(\tilde{q})$ . So the magnitude of  $q_{tt}$  is directly impacted by the initial Lorenz curve. This can be seen in Fig. 3 following the green dashed lines. In Fig. 3(b) the first point is at 0.27 on the vertical axis, which is the highest possible point below the blue curve for  $x = e^{-\beta E_{tt}}$ . This value indeed corresponds to the quantum yield  $QY_{\text{both}} = 0.27$  [and the same for Fig. 3(a) where  $QY_{\text{both}} = 0.39$ ].



(a) **High coherence**, with initial state:  $\vec{p}_{sup}(p = 0.7, \lambda = 0.2)$ .



(b) **Low coherence**, with initial state:  $\vec{p}_{sup}(p = 0.7, \lambda = 0.02)$ .

FIG. 3. Effect of coherences on quantum yield. The figures show an initial state (blue) and below its final states that maximize the quantum yield whether it is defined as  $QY_{any}$  (purple) or  $QY_{both}$  (green dotted). Higher coherence [Fig. 3(a)] leads to higher quantum yields, see  $QY_{both}$ .

To summarize, the higher the initial coherence, the higher the initial Lorenz curve, the more possibilities for the final curve and the higher its quantum yield.

The figure also presents the other possible definition of the quantum yield. For  $\lambda = 0.02$  and for  $\lambda = 0.2$  the optimal is  $QY_{any} = 0.81$ . The increase in coherence does not seem to affect this definition of the quantum yield at first sight, but this is not true for all energy values.

In Fig. 4 we show the best possible quantum yield one can obtain with thermomajorization as a function of the energy gap  $\Delta E$  between the two ground states  $|g\rangle$  (*cis*) and  $|t\rangle$  (*trans*). The darker colors show results where the initial

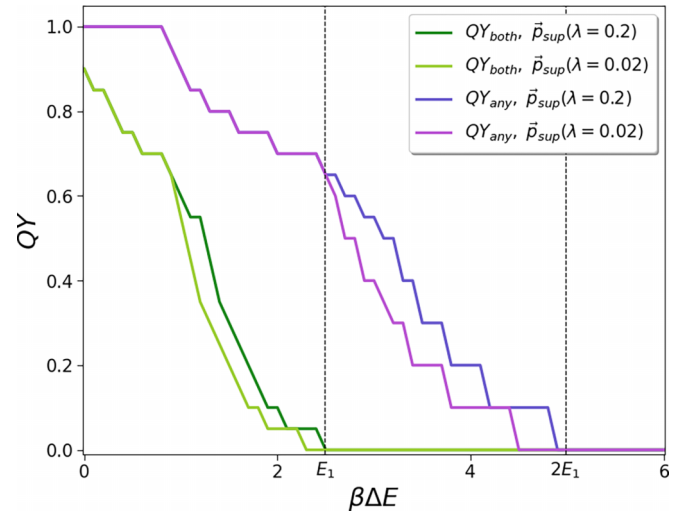


FIG. 4. Quantum yields as a function of energy gap by superposing two excited molecules. Different definitions of quantum yield:  $QY_{both}$  (green) and  $QY_{any}$  (purple). Initial  $\vec{p}_{sup}$  as in Eq. (31). All curves plotted with  $p = 0.7$ . Dark colors represent higher initial coherence ( $\lambda = 0.2$ ), lighter colors have lower coherence ( $\lambda = 0.02$ ) (accordingly they have lower quantum yields).

state corresponds to  $\lambda = 0.2$ , and the lighter ones to  $\lambda = 0.02$ . The purple curves correspond to the  $QY_{any}$  definition of the quantum yield, while the green ones show the optimal  $QY_{both}$ . In both cases, the darker line remains above the lighter one, because higher coherence induces a higher optimal quantum yield independently of which definition we choose. A hierarchy exists among these definitions, since  $QY_{any}$  contains more terms, it will always be higher than  $QY_{both}$ .

The curves appear step-like due to the sampling resolution along the vertical axis resulting from high computational overhead. The simulation evaluates all possible population vectors in a vector space with dimension  $3^2 = 9$  and checks whether they have the highest quantum yield, and are thermomajorized by the initial state.

The dotted vertical lines show when the energy gap  $\Delta E$  equals  $E_1$  and  $2E_1$ . These energies are related to states where one molecule is excited, or both, respectively. The lines correspond to the cusp where  $QY_{any}$  begin to decrease. When the energy gap is larger than the initial excitations it becomes harder to reach the *trans* state. So there is an exponential decrease of the quantum yield with increasing  $\Delta E$ . At  $\Delta E > E_1$ , states with a single excited molecule can no longer access to the *trans* state, so now the quantum yield takes lower values. Finally, when  $\Delta E$  exceeds double the excitation energy, it becomes impossible for any initial state to reach the *trans* state and the quantum yield tends to zero. However, as mentioned earlier,  $QY_{any}$  is always higher than  $QY_{both}$  (in green) regardless the initial coherence, because photoisomerizing both molecules takes twice the energy. Indeed, the green curves already start decreasing towards zero at  $\Delta E \approx E_1$  instead of  $2E_1$  like the purple ones. Interestingly, coherence does not have the same effect for all values of  $\Delta E$ . To illustrate the intricate dependency on multiple parameters, Fig. 5 shows the increase of the quantum yield  $QY_{any}$  as a function of both the initial probability  $p$  and

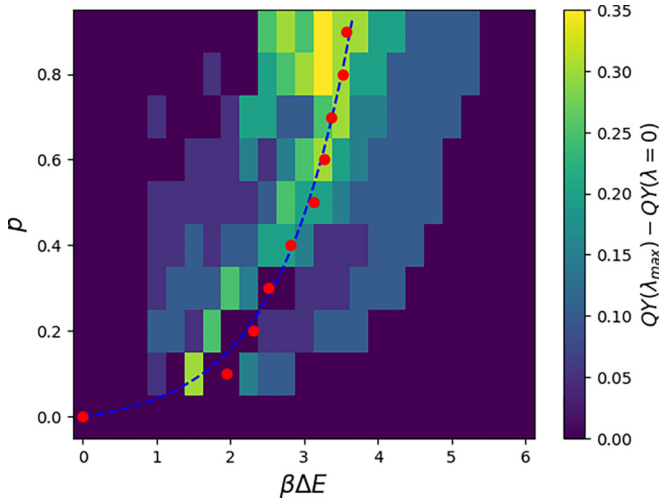


FIG. 5. The increase of quantum yield  $QY_{\text{asy}}$  as a function of excitation probability  $p$  and  $\beta\Delta E$ . It corresponds to the difference of  $QY_{\text{asy}}$  between the maximally coherent and noncoherent case. The red points indicate for each  $p$  the average  $\Delta E$  where the difference is maximal. The blue dotted line is the fitted curve  $p = f(\beta\Delta E) = p_0(e^{\beta\Delta E} - 1)$  passing through these points.

the energy gap  $\Delta E$ . The plotted quantity is the difference between the case where the states are maximally coherent,  $\lambda_{\text{max}} = p/2$ , and the incoherent case,  $\lambda = 0$ :  $QY_{\text{asy}}(\lambda_{\text{max}}) - QY_{\text{asy}}(\lambda = 0)$ . Due to the important computational overhead, the figure is coarse-grained. However one can clearly distinguish a line  $p = f(\beta\Delta E)$  where the effect of coherence is the strongest. The average points of maximal effect (in red) seem to fit an exponential curve  $f(\beta\Delta E) = p_0(e^{\beta\Delta E} - 1)$  (in blue) where  $p_0 \approx 0.025$ . It will be the task of subsequent work to analyze this dependence exactly and to explain its origin.

The results in this study were obtained for  $\beta = 1 \text{ eV}^{-1}$  corresponding to unphysical temperatures limiting physical insight into photoisomerization. If one works at room temperature ( $\beta = 38.9 \text{ eV}^{-1}$ ), the exponential decrease of Fig. 4 becomes very sharp, because the energy levels are too far apart compared with the thermal excitations. In other words, a cold thermal bath cannot facilitate transitions from lower to higher-lying states. This leads to a limited quantum yield; indeed, to

optimize the quantum yield, some of the population of the *cis* ground state must be able to transition towards the *trans* configuration. This can be remedied by using molecules which have lower transition energies than rhodopsin. The advantage of using rhodopsin as a test case is that its state energies benefit from extensive characterization. We are investigating other photoswitchable molecules [38] to extend the scope of this work.

## V. CONCLUSION

In general, quantum thermodynamical models avoid the high-temperature limit. However, this work finds that higher temperatures enable transitions to higher-energy states that are inaccessible at lower temperatures. Real systems are more complicated. The discrete energy levels considered here correspond in reality to broad continuous absorption peaks. To capture the intricate dynamics of complex molecular switches and accurately assess the influence of coherence on photoisomerization yield, a more sophisticated environmental modelization—such as an open systems approach—could prove indispensable. A particularly interesting case study is rhodopsin, which benefits from advanced simulation techniques [39,40] and is of wide interest for biochemical applications [41–43]. There are hints of the importance coherence during the photoisomerizing process [34,44]. Our methodology of considering the role of coherence and thermomajorization could in principle help to estimate the efficiency of photoisomerization and to gain a deeper understanding of its drivers. In future works it could be interesting to relate coherence to other types of resources like classical and quantum correlations.

## ACKNOWLEDGMENTS

We thank Prof. M. Olivucci and Dr. L. Pedraza-González for helpful discussions on their simulations of rhodopsin and for sharing simulated parameters. T.F. thanks the Gordon and Betty Moore Foundation, Lillian Martin and the Oxford Martin School, and the John Fell Fund for support. O.P. acknowledges support by the Scientific and Technological Research Council of Turkey (TUBITAK) under Grant No. 120F089. M.B. thanks the ENS Paris-Saclay ARPE programme for support.

- [1] J. Goold, M. Huber, A. Riera, L. d. Rio, and P. Skrzypczyk, *J. Phys. A: Math. Theor.* **49**, 143001 (2016).
- [2] S. Vinjanampathy and J. Anders, *Contemp. Phys.* **57**, 545 (2016).
- [3] *Thermodynamics in the Quantum Regime: Fundamental Aspects and New Directions*, edited by F. Binder, L. A. Correa, C. Gogolin, J. Anders, and G. Adesso (Springer International Publishing, Cham, 2018).
- [4] S. Deffner and S. Campbell, *Quantum Thermodynamics* (Morgan & Claypool Publishers, 2019).
- [5] R. Alicki and R. Kosloff, Introduction to quantum thermodynamics: History and prospects, in *Thermodynamics in the Quantum Regime: Fundamental Aspects and New Directions*,

- edited by F. Binder, L. A. Correa, C. Gogolin, J. Anders, and G. Adesso (Springer International Publishing, Cham, 2018), pp. 1–33.
- [6] H. P. Breuer and F. Petruccione, *The Theory of Open Quantum Systems*, 1st ed. (Oxford University Press, 2002), Chap. 3, pp. 130–137.
- [7] W. K. Wootters and W. H. Zurek, *Nature (London)* **299**, 802 (1982).
- [8] G. Gour, M. P. Müller, V. Narasimhachar, R. W. Spekkens, and N. Y. Halpern, *Phys. Rep.* **583**, 1 (2015).
- [9] N. H. Y. Ng and M. P. Woods, Resource theory of quantum thermodynamics: Thermal operations and second laws, in *Thermodynamics in the Quantum Regime: Fundamental Aspects and*

- New Directions*, edited by F. Binder, L. A. Correa, C. Gogolin, J. Anders, and G. Adesso (Springer International Publishing, Cham, 2018), pp. 625–650.
- [10] M. Lostaglio, *Rep. Prog. Phys.* **82**, 114001 (2019).
- [11] G. Torun, O. Pusuluk, and O. E. Müstecaplıoğlu, *Turk. J. Phys.* **47**, 141 (2023).
- [12] B. Coecke, T. Fritz, and R. W. Spekkens, *Inf. Comput. Quantum Phys. Log.*, **250**, 59 (2016).
- [13] E. Chitambar and G. Gour, *Rev. Mod. Phys.* **91**, 025001 (2019).
- [14] J. B. Brask, G. Haack, N. Brunner, and M. Huber, *New J. Phys.* **17**, 113029 (2015).
- [15] B. Çakmak, A. Manatuly, and O. E. Müstecaplıoğlu, *Phys. Rev. A* **96**, 032117 (2017).
- [16] I. Henao and R. M. Serra, *Phys. Rev. E* **97**, 062105 (2018).
- [17] G. Manzano, R. Silva, and J. M. R. Parrondo, *Phys. Rev. E* **99**, 042135 (2019).
- [18] A. Tavakoli, G. Haack, N. Brunner, and J. B. Brask, *Phys. Rev. A* **101**, 012315 (2020).
- [19] A. Tuncer and O. Müstecaplıoğlu, *Turk. J. Phys.* **44**, 404 (2020).
- [20] C. Dağ, W. Niedenzu, O. E. Müstecaplıoğlu, and G. Kurizki, *Entropy* **18**, 244 (2016).
- [21] A. Manatuly, W. Niedenzu, R. Román-Ancheyta, B. Çakmak, O. E. Müstecaplıoğlu, and G. Kurizki, *Phys. Rev. E* **99**, 042145 (2019).
- [22] C. L. Latune, I. Sinayskiy, and F. Petruccione, *Phys. Rev. Res.* **1**, 033097 (2019).
- [23] C. L. Latune, I. Sinayskiy, and F. Petruccione, *Sci. Rep.* **9**, 3191 (2019).
- [24] C. L. Latune, I. Sinayskiy, and F. Petruccione, *Phys. Rev. A* **102**, 042220 (2020).
- [25] O. Pusuluk and O. E. Müstecaplıoğlu, *Phys. Rev. Res.* **3**, 023235 (2021).
- [26] M. Lostaglio, K. Korzekwa, D. Jennings, and T. Rudolph, *Phys. Rev. X* **5**, 021001 (2015).
- [27] G. Gour, D. Jennings, F. Buscemi, R. Duan, and I. Marvian, *Nat. Commun.* **9**, 5352 (2018).
- [28] T. Biswas, A. d. O. Junior, M. Horodecki, and K. Korzekwa, *Phys. Rev. E* **105**, 054127 (2022).
- [29] N. Yunger Halpern and D. T. Limmer, *Phys. Rev. A* **101**, 042116 (2020).
- [30] G. Spaventa, S. F. Huelga, and M. B. Plenio, *Phys. Rev. A* **105**, 012420 (2022).
- [31] M. Horodecki and J. Oppenheim, *Nat. Commun.* **4**, 2059 (2013).
- [32] O. P. Ernst, D. T. Lodowski, M. Elstner, P. Hegemann, L. S. Brown, and H. Kandori, *Chem. Rev. (Washington, DC, US)* **114**, 126 (2014).
- [33] S. Hahn and G. Stock, *J. Phys. Chem. B* **104**, 1146 (2000).
- [34] Q. Wang, R. W. Schoenlein, L. A. Peteanu, R. A. Mathies, and C. V. Shank, *Science* **266**, 422 (1994).
- [35] O. Pusuluk, T. Farrow, C. Deliduman, K. Burnett, and V. Vedral, *Proc. R. Soc. London A* **474**, 20180037 (2018).
- [36] P. J. M. Johnson, M. H. Farag, A. Halpin, T. Morizumi, V. I. Prokhorenko, J. Knoester, T. L. C. Jansen, O. P. Ernst, and R. J. D. Miller, *J. Phys. Chem. B* **121**, 4040 (2017).
- [37] L. Pedraza-González, L. De Vico, M. d. C. Marín, F. Fanelli, and M. Olivucci, *J. Chem. Theory Comput.* **15**, 3134 (2019).
- [38] A. E. Hillers-Bendtsen, J. L. Elholm, O. B. Obel, H. Hölzel, K. Moth-Poulsen, and K. V. Mikkelsen, *Angew. Chem. Int. Ed.* **62**, e202309543 (2023).
- [39] X. Yang, M. Manathunga, S. Gozem, J. Léonard, T. Andruniów, and M. Olivucci, *Nat. Chem.* **14**, 441 (2022).
- [40] L. Pedraza-González, L. Barneschi, D. Padula, L. De Vico, and M. Olivucci, *Top. Curr. Chem.* **380**, 21 (2022).
- [41] M. Kurihara and Y. Sudo, *Biophys. Physicobiol.* **12**, 121 (2015).
- [42] K. Kojima, A. Shibukawa, and Y. Sudo, *Biochemistry* **59**, 218 (2020).
- [43] H. Kandori, *Bull. Chem. Soc. Jpn.* **93**, 76 (2020).
- [44] V. I. Prokhorenko, A. M. Nagy, S. A. Waschuk, L. S. Brown, R. R. Birge, and R. J. D. Miller, *Science* **313**, 1257 (2006).